

Article

Performance Analysis of Optical Spatial Modulation in Atmospheric Turbulence Channel

Hammed G. Olanrewaju ^{1,†,‡}, John Thompson ^{2,†,‡} and Wasiu O. Popoola ^{3,†,‡*}

¹ g.olaneawaju@ed.ac.uk

² john.thompson@ed.ac.uk

³ w.popoola@ed.ac.uk

* Correspondence: w.popoola@ed.ac.uk

† School of Engineering, Institute for Digital Communications, LiFi R&D Centre, University of Edinburgh, United Kingdom.

‡ These authors contributed equally to this work.

§ Invited Paper

Abstract: In this paper, spatial pulse position modulation (SPPM) is used as a case study to investigate the performance of the optical spatial modulation (SM) technique in outdoor atmospheric turbulence (AT). A closed-form expression for the upper bound on the asymptotic symbol error rate (SER) of SPPM in AT is derived and validated by closely-matching simulation results. The error performance is evaluated in weak to strong AT conditions. As the AT strength increases from the weak to strong, the channel fading coefficients become more dispersed and differentiable. Thus, a better error performance is observed under moderate-to-strong AT compared to weak AT. The performance in weak AT can be improved by applying unequal power allocation to make FSO links more distinguishable at the receiver. Receive diversity is considered to mitigate irradiance fluctuation and improve the robustness of the system to turbulence-induced channel fading. The diversity order is computed as half of the number of detectors. Performance comparisons, in terms of energy and spectral efficiencies, are drawn between the SPPM scheme and conventional MIMO schemes such as repetition coding and spatial multiplexing.

Keywords: optical communications; optical spatial modulation; free-space optical communication; multiple-input-multiple-output (MIMO) systems; pulse position modulation; atmospheric turbulence.

1. Introduction

Free-space optical communication (FSO) technology is a promising complement to existing radio frequency communications. In addition to its huge bandwidth resource and its potential to support gigabit rate throughput, the FSO system can be deployed using low-power and low-cost components [1,2]. The major drawback of the FSO technology is its dependence on atmospheric conditions, which affects link availability. Variations in pressure and temperature create random changes in the refractive index of the atmosphere. This leads to atmospheric turbulence (AT) induced fluctuation in the received irradiance [3–5].

In order to enhance capacity, reliability and/or coverage, multiple-input multiple-output (MIMO) techniques are employed to exploit additional degrees of freedom, such as the space and emitted colour of the optical sources and the field of view of the detectors. FSO systems using MIMO diversity techniques are explored in [4,6,7] to mitigate the effect of turbulence-induced fading by providing redundancy. In this paper, we consider the use of a low-complexity MIMO technique known as spatial modulation (SM) [8,9], to enhance the spectral efficiency of FSO systems. The SM technique achieves higher spectral efficiency by encoding additional information bits in the spatial domain of the multiple optical sources at the transmitter.

Multiple variants of SM have been explored in FSO systems, using different statistical distributions to model the channel fading [10–15]. A variant of optical SM (OSM) termed space shift keying (SSK) is

34 studied in [10–12]. In the SSK scheme, no digital signal modulation is used, and the information bits are
35 encoded solely on the spatial index of the optical sources. Our paper differs from these previous works
36 in that we have considered a full-fledged OSM scheme which entails using both the spatial index of the
37 sources and the transmitted digital signal modulation to convey the information bits. The work in [13]
38 is related to ours, as it considered an OSM scheme in which digital signal modulation is also employed.
39 However, the analytical framework includes kernel density estimation which does not provide a
40 closed-form solution. Using the Homodyned-K (HK) distribution to model turbulence-induced fading,
41 the performance of outdoor OSM (SSK) with coherent detection is reported in [14]. Also, [16] considers
42 power series based analysis of effect of misalignment and Gamma–Gamma turbulence fading on the
43 SM technique with BPSK constellation

44 Given that AT primarily affects the emitted light intensity, pulse position modulation (PPM)
45 is commonly used in an FSO system because, unlike on-off keying (OOK) and pulse-amplitude
46 modulation (PAM), its detection process is not reliant on the channel states [3]. Nevertheless, PPM
47 is limited by its high bandwidth requirement. In order to enhance the spectral efficiency of PPM, a
48 variant of the OSM technique termed spatial pulse position modulation (SPPM) [17] is explored in this
49 paper. SPPM also benefits from the power efficiency of the PPM technique. The intensity fluctuations
50 caused by AT is modelled by the Gamma-Gamma (GG) distribution, which is widely adopted to study
51 FSO links under weak to strong AT conditions because it matches experimental results [1,18].

52 In this work, the performance of an SPPM-based FSO system is evaluated under weak to strong
53 AT conditions. The contributions of this paper include: (1) the theoretical expression for the upper
54 bound on the asymptotic symbol error rate (SER) of SPPM in FSO channels is derived and validated
55 by closely matching simulation results. (2) As the AT strength increases from the weak to strong,
56 the distribution of the fading coefficients spreads out more. Thus, the influence of the dispersion
57 of the coefficients on error performance of OSM schemes is explored under different AT conditions.
58 (3) Furthermore, since SM provides increased throughput but not transmit diversity gain, spatial
59 diversity is considered at the receiver in order to improve the system performance, and the diversity
60 gain of the multiple-detector system is obtained from the error plots. (4) The performance of the SPPM
61 scheme is also compared to that of SSK and other conventional MIMO schemes such as repetition
62 coding (RC) and spatial multiplexing (SMUX). The performance comparison is presented in terms of
63 energy and spectral efficiencies.

64 The rest of the paper is organized as follows. The system and channel models are provided in
65 Section 2. In Section 3, the theoretical derivation of the upper bound on asymptotic SER of SPPM in
66 GG FSO channels is presented. The results of the performance evaluation are provided and discussed
67 in Section 4, and our concluding remarks are given in Section 5.

68 2. System and Channel Model

69 2.1. The SPPM Scheme

70 Considering an $N_t \times N_r$ optical MIMO system with N_t optical transmit units (TXs), i.e., light
71 emitting diodes (LEDs) or lasers and N_r receive units (RXs), i.e., PIN photodetectors (PD), by using the
72 SPPM scheme [17], only one of the TXs is activated in a given symbol duration, while the rest of the
73 TXs are idle. The activated source transmits an L -PPM signal pattern, where L denotes the number of
74 time slots (chips) in a symbol duration. A total of $M = \log_2(N_t L)$ bits are transmitted per data symbol.
75 The first $\log_2(N_t)$ most significant bits are encoded in the index (position) of the activated TX while the
76 remaining $\log_2(L)$ bits are conveyed by the pulse position in the transmitted PPM signal. The SPPM
77 encoding is further illustrated in Figure 1 for the case of $N_t = 4$ and $L = 4$. For instance, to transmit the
78 symbol ‘13’ with binary representation ‘1101’, the two most significant bits, ‘11’, are used to select ‘TX
79 4’, while the last two bits, ‘01’, indicate that the pulse will be transmitted in the second time slot of the
80 4-PPM pulse pattern.

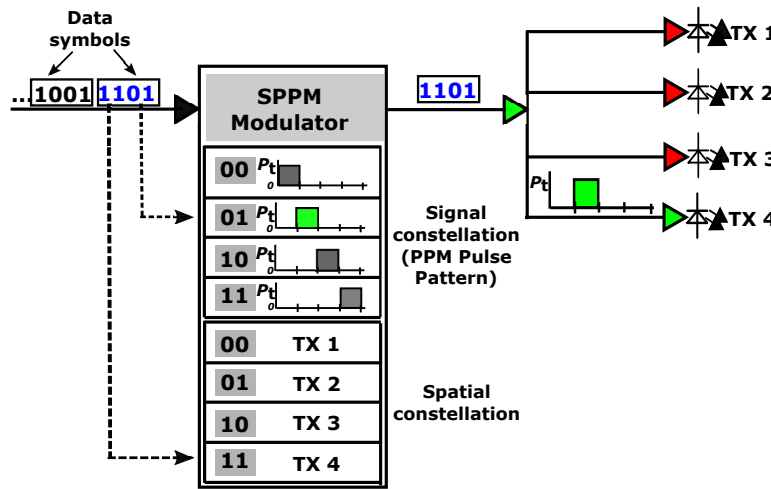


Figure 1. Illustration of SPPM encoding using $N_t = 4$, $L = 4$.

2.2. SPPM System Model

Consider that a data symbol is transmitted by activating the j th LED, $1 \leq j \leq N_t$, to transmit a pulse in slot m , $0 \leq m \leq (L - 1)$, of the L -PPM signal, the $N_r \times 1$ vector of received electrical signal over the symbol duration, T , is:

$$\mathbf{r}(t) = \omega_j R \mathbf{H} \mathbf{s}_{j,m}(t) + \mathbf{n}(t), \quad 0 \leq t \leq T, \quad (1)$$

where R is the responsivity of the PD. The parameter ω_j for $j = 1, \dots, N_t$, are weights which can be applied to induce power imbalance between the TXs in order to improve their differentiability at the receiver. The $N_r \times N_t$ FSO channel matrix is represented by \mathbf{H} . The quantity $\mathbf{n}(t)$ is the sum of the ambient light shot noise and the thermal noise in the N_r PIN PDs, and it is modelled as independent and identically distributed (i.i.d) additive white Gaussian noise (AWGN) with variance $\sigma^2 = N_0/2$; N_0 represents the noise power spectral density [1,19]. The $N_t \times 1$ transmit signal vector, $\mathbf{s}_{j,m}(t) = [0, \dots, s_{j,m}(t), \dots, 0]^T$, has a nonzero entry at the index of the activated j th TX, where T denotes the transpose operation, and $s_{j,m}(t)$ is the transmitted L -PPM waveform, with a pulse of amplitude P_t in slot m .

The matched filter (MF) receiver architecture employs a unit-energy receive filter, and the output of the MF in each time slot is obtained by sampling at the chip rate, $1/T_c$, where the duration of each time slot, $T_c = T/L$. Based on the maximum likelihood (ML) detection criterion, the estimate of the transmitted SPPM symbol is obtained from the combination of the pulse position and the TX index which gives the minimum Euclidean distance from the received signal [17]. That is,

$$[\hat{m}, \hat{j}] = \arg \max_{m, j} f_r(\mathbf{r} | \mathbf{s}_{j,m}, \omega_j, \mathbf{H}), \quad (2)$$

where $f_r(\mathbf{r} | \mathbf{s}_{j,m}, \omega_j, \mathbf{H})$ is the probability density function (PDF) of \mathbf{r} conditioned on $\mathbf{s}_{j,m}$ being transmitted, weight ω_j and channel matrix \mathbf{H} .

2.3. FSO Channel Model

As the transmitted signal propagates through the FSO channel, it experiences turbulence-induced channel fading which is characterised by the GG distribution [1,20]. The PDF of the GG fading coefficients is given by [20]:

$$f_H(h) = \frac{2(\alpha\beta)^{\frac{\alpha+\beta}{2}}}{\Gamma(\alpha)\Gamma(\beta)} h^{\frac{\alpha+\beta}{2}-1} K_{\alpha-\beta}(2\sqrt{\alpha\beta}h) \quad (3)$$

where h is the fading coefficient. The functions $\Gamma(\cdot)$ and $K_\nu(\cdot)$ denote the Gamma function and the modified Bessel function of the second kind of order ν , respectively. The scalars α and β are the scintillation parameters that characterize the intensity fluctuations, and they are related to the atmospheric conditions through the log-intensity variance σ_l^2 . The values of α , β and σ_l^2 specified for different regimes of atmospheric turbulence are given in Table 1 from [1].

Table 1. Atmospheric turbulence parameters [1].

Turbulence Level	σ_l^2	α	β
Weak	0.2	11.7	10.1
Moderate	1.6	4.0	1.9
Strong	3.5	4.2	1.4

In order to provide a closed-form solution, the modified Bessel function in (3) is expressed in terms of the Meijer-G function, $G_{c,d}^{a,b}(\cdot)$ by applying [21, (8.4.23.1)]:

$$K_{\alpha-\beta}(2\sqrt{\alpha\beta h}) = \frac{1}{2} G_{0,2}^{2,0} \left(\alpha\beta h \left| \begin{smallmatrix} \alpha-\beta & - \\ \frac{\alpha-\beta}{2} & \frac{\beta-\alpha}{2} \end{smallmatrix} \right. \right), \quad (4)$$

to obtain:

$$f_H(h) = \frac{(\alpha\beta)^{\frac{\alpha+\beta}{2}}}{\Gamma(\alpha)\Gamma(\beta)} h^{\frac{\alpha+\beta}{2}-1} G_{0,2}^{2,0} \left(\alpha\beta h \left| \begin{smallmatrix} \alpha-\beta & - \\ \frac{\alpha-\beta}{2} & \frac{\beta-\alpha}{2} \end{smallmatrix} \right. \right). \quad (5)$$

To further simplify (5), we utilize [21, (8.2.2.15)]:

$$Z^\alpha G_{p,q}^{m,n} \left(z \left| \begin{smallmatrix} (a_p) & \\ (bq) & \end{smallmatrix} \right. \right) = G_{p,q}^{m,n} \left(z \left| \begin{smallmatrix} (a_p)+\alpha & \\ (bq)+\alpha & \end{smallmatrix} \right. \right), \quad (6)$$

and the expression (5) is reduced to:

$$f_H(h) = \frac{(\alpha\beta)}{\Gamma(\alpha)\Gamma(\beta)} G_{0,2}^{2,0} \left(\alpha\beta h \left| \begin{smallmatrix} - & \\ \alpha-1, \beta-1 & \end{smallmatrix} \right. \right). \quad (7)$$

It is assumed that the individual units in the transmitter and receiver arrays are spatially separated by at least the correlation width, $w_c = \sqrt{\lambda d}$, such that the elements of the FSO channel matrix, \mathbf{H} , are independent and uncorrelated. The transmission wavelength and the link distance are denoted by λ and d respectively. This assumption is realistic because the transverse correlation width of the laser radiation in AT is typically on the order of a few centimeters [5,22]. For instance, in an FSO system with $\lambda = 1.55 \mu\text{m}$ and link distance of $d = 2.5 \text{ km}$, for the received signals to be uncorrelated, the required spatial spacing is about $w_c = 6.2 \text{ cm}$. Thus, we can infer that the proposed system model can be implemented with practical spacings between each unit of the transmit and receive arrays.

3. Performance Analysis of SPPM in FSO

As stated in Section 2.2, a transmitted data symbol is correctly detected if both the pulse position and the TX index are correctly detected. Thus, the symbol error probability of SPPM is given by:

$$P_{e,\text{sym}} = 1 - (P_{c,\text{tx}} \times P_{c,\text{ppm}}), \quad (8)$$

where $P_{c,\text{ppm}}$ is the probability of correctly detecting the PPM pulse position and $P_{c,\text{tx}}$ is the probability of correctly detecting the index of the activated TX given that pulse position has been correctly detected. The expressions for $P_{c,\text{ppm}}$ and $P_{c,\text{tx}}$ are derived as follows.

111 3.1. Probability of Correct Transmitter Detection

Consider that the transmitted data symbol is sent by activating TX j . For a correctly detected pulse position, the pairwise error probability (PEP) that the receiver decides in favour of TX i instead of j , is given by [17]:

$$\text{PEP}_m^{j \rightarrow i} = \frac{1}{2} \text{erfc} \left(\frac{\sqrt{\gamma_s}}{2} \sum_{k=1}^{N_r} \left| \omega_i h_{ik} - \omega_j h_{jk} \right| \right), \quad (9)$$

112 where $\text{erfc}(\cdot)$ denotes the complementary error function. The scalars h_{ik} and h_{jk} for $1 \leq i, j \leq N_t$,
 113 are the channel fading coefficients of the link between the k th PD and the TXs i and j respectively.
 114 The signal-to-noise ratio (SNR) per symbol, $\gamma_s = E_s / N_0$, and the average energy per symbol, $E_s =$
 115 $(RP_t)^2 T_c$.

To simplify the analyses that will follow, we define the following random variables (RV): $U_k = \omega_i h_{ik}$, $V_k = \omega_j h_{jk}$, and $X_k = U_k - V_k$. Also, we define $Y_k = |X_k|$, $Z_k = Y_k^2 \gamma_s$, and $\psi = \sum_{k=1}^{N_r} Z_k$. Therefore, equation (9) becomes:

$$\text{PEP}_m^{j \rightarrow i} = \frac{1}{2} \text{erfc} \left(\frac{\sqrt{\psi}}{2} \right). \quad (10)$$

Furthermore, the expression in (10) represents the instantaneous PEP conditioned on the random variable ψ . Therefore, by averaging over the PDF of ψ , the average PEP is obtained as:

$$\text{APEP}_m^{j \rightarrow i} = \frac{1}{2} \int_0^\infty \text{erfc} \left(\frac{\sqrt{\psi}}{2} \right) f_\psi(\psi) d\psi. \quad (11)$$

116 The PDF of ψ , as well as the $\text{APEP}_m^{j \rightarrow i}$, is obtained as follows.

The random variable, X_k , is a function of two independent, identically distributed and non-negative GG random variables, h_{ik} and h_{jk} , whose PDF is given by (7). By the transformation of RV, the PDF of X_k is obtained as:

$$f_{X_k}(x_k) = \begin{cases} \int_{-x_k}^{\infty} f_{U_k}(x_k + v_k) f_{V_k}(v_k) dv_k; & \text{for } x_k < 0 \\ \int_0^{\infty} f_{U_k}(x_k + v_k) f_{V_k}(v_k) dv_k; & \text{for } x_k \geq 0. \end{cases} \quad (12)$$

Considering the first case in (12), i.e., $x_k < 0$, by using the variable substitution: $\tau = v_k + x_k$, we obtain:

$$f_{X_k}(x_k) = \int_0^{\infty} f_{U_k}(\tau) f_{V_k}(\tau - x_k) d\tau \quad \text{for } x_k < 0. \quad (13)$$

The PDFs f_{U_k} and f_{V_k} of the RVs U_k and V_k respectively, are derived from (7), and they are applied in (13) to express the PDF of the RV X_k as:

$$f_{X_k}(x_k) = \frac{(\alpha\beta)^2}{\omega_i \omega_j (\Gamma(\alpha)\Gamma(\beta))^2} \int_0^{\infty} G_{0,2}^{2,0} \left(\frac{\alpha\beta\tau}{\omega_i} \middle| {}_{\alpha-1, \beta-1} \right) G_{0,2}^{2,0} \left(\frac{\alpha\beta(\tau - x_k)}{\omega_j} \middle| {}_{\alpha-1, \beta-1} \right) d\tau. \quad (14)$$

Also, the transformation in [21, (2.24.1.3)] is employed to solve the integral of the product of two Meijer-G terms, and thus, (14) reduces to:

$$f_{X_k}(x_k) = \frac{\alpha\beta}{\omega_i (\Gamma(\alpha)\Gamma(\beta))^2} \sum_{\lambda=0}^{\infty} \frac{(x_k)^\lambda}{\lambda!} G_{3,3}^{2,3} \left(\frac{\omega_j}{\omega_i} \middle| {}_{\alpha-1, \beta-1, \lambda}^{0, 1+\lambda-\alpha, 1+\lambda-\beta} \right). \quad (15)$$

117 Similarly, for the second case in (12), i.e., $x_k \geq 0$, by using (7) and [21, (2.24.1.3)], the expression
 118 obtained for $f_{X_k}(x_k)$ is the same as that given in (15).

Now, the PDF of Y_k is given by:

$$f_{Y_k}(y_k) = f_{X_k}(y_k) + f_{X_k}(-y_k) \quad \text{for } y_k > 0. \quad (16)$$

Since Y_k is an absolute value function, then $y_k > 0 \forall k$. Thus, $f_{X_k}(y_k) = f_{X_k}(x_k)$ for $x_k \geq 0$ and $f_{X_k}(-y_k) = f_{X_k}(x_k)$ for $x_k < 0$ as defined by (12). Hence, from (16), the PDF of Y_k is given by:

$$\begin{aligned} f_{Y_k}(y_k) &= 2f_{X_k}(y_k) \\ &= \frac{2\alpha\beta}{\omega_i(\Gamma(\alpha)\Gamma(\beta))^2} \sum_{\lambda=0}^{\infty} \frac{(y_k)^\lambda}{\lambda!} G_{3,3}^{2,3} \left(\frac{\omega_j}{\omega_i} \middle| \begin{smallmatrix} 0,1+\lambda-\alpha,1+\lambda-\beta \\ \alpha-1,\beta-1,\lambda \end{smallmatrix} \right). \end{aligned} \quad (17)$$

Using RV transformation between variables Y_k and Z_k , the PDF of Z_k can be expressed as:

$$\begin{aligned} f_{Z_k}(z_k) &= \frac{1}{2\sqrt{z_k\gamma_s}} f_{Y_k} \left(\sqrt{z_k/\gamma_s} \right) \\ &= \frac{\alpha\beta}{\omega_i(\Gamma(\alpha)\Gamma(\beta))^2} \sum_{\lambda=0}^{\infty} \frac{(z_k)^{\frac{\lambda-1}{2}}}{\lambda! (\sqrt{\gamma_s})^{\lambda+1}} \times G_{3,3}^{2,3} \left(\frac{\omega_j}{\omega_i} \middle| \begin{smallmatrix} 0,1+\lambda-\alpha,1+\lambda-\beta \\ \alpha-1,\beta-1,\lambda \end{smallmatrix} \right). \end{aligned} \quad (18)$$

As defined above, the random variable ψ is a sum of N_r i.i.d realizations of variable Z_k . Therefore, to obtain the PDF of ψ , we first derive the moment generating function (MGF) of Z_k . Using the the asymptotic PDF of Z_k , which is obtained by substituting $\lambda=0$ in (18), the MGF of Z_k is obtained as:

$$\begin{aligned} M_{Z_k}(s) &= \int_0^{\infty} e^{-sz_k} \left[f_{Z_k}(z_k) \Big|_{\lambda=0} \right] dz_k \\ &= \frac{\alpha\beta}{\omega_i(\Gamma(\alpha)\Gamma(\beta))^2 \sqrt{\gamma_s}} G_{3,3}^{2,3} \left(\frac{\omega_j}{\omega_i} \middle| \begin{smallmatrix} 0,1-\alpha,1-\beta \\ \alpha-1,\beta-1,0 \end{smallmatrix} \right) \times \int_0^{\infty} \frac{e^{-sz_k}}{\sqrt{(z_k)}} dz_k \\ &= \frac{\alpha\beta\sqrt{\pi}}{\omega_i(\Gamma(\alpha)\Gamma(\beta))^2 \sqrt{s\gamma_s}} G_{3,3}^{2,3} \left(\frac{\omega_j}{\omega_i} \middle| \begin{smallmatrix} 0,1-\alpha,1-\beta \\ \alpha-1,\beta-1,0 \end{smallmatrix} \right). \end{aligned} \quad (19)$$

From (19), the MGF of the ψ is given by:

$$\begin{aligned} M_{\psi}(s) &= \prod_{k=1}^{N_r} M_{Z_k}(s) \\ &= \left[\frac{\alpha\beta\sqrt{\pi s}}{\omega_i(\Gamma(\alpha)\Gamma(\beta))^2 \sqrt{\gamma_s}} G_{3,3}^{2,3} \left(\frac{\omega_j}{\omega_i} \middle| \begin{smallmatrix} 0,1-\alpha,1-\beta \\ \alpha-1,\beta-1,0 \end{smallmatrix} \right) \right]^{N_r}. \end{aligned} \quad (20)$$

The PDF of the random variable ψ is obtained from the inverse Laplace transform of $M_{\psi}(s)$ as:

$$f_{\psi}(\psi) = \frac{\psi^{(\frac{N_r}{2}-1)}}{\Gamma(\frac{N_r}{2})} \left(\frac{\alpha\beta\sqrt{\pi}(\gamma_s)^{-\frac{1}{2}}}{\omega_i(\Gamma(\alpha)\Gamma(\beta))^2} G_{3,3}^{2,3} \left(\frac{\omega_j}{\omega_i} \middle| \begin{smallmatrix} 0,1-\alpha,1-\beta \\ \alpha-1,\beta-1,0 \end{smallmatrix} \right) \right)^{N_r}. \quad (21)$$

By substituting (21) in (11), and applying the integral relation [23, (4.1.18)]:

$$\int_0^{\infty} \text{erfc}(ax)x^p dx = \frac{1}{(p+1)a^{p+1}\sqrt{\pi}} \Gamma \left(\frac{p}{2} + 1 \right), \quad (22)$$

for $|\arg\{a\}| < \pi/4$, $p < -1$, the asymptotic PEP of detecting the index of the activated TX is given by:

$$\text{APEP}_m^{j \rightarrow i} = \frac{2^{N_r} \Gamma(\frac{N_r+1}{2})}{N_r \Gamma(\frac{N_r}{2})} \left(\frac{\alpha\beta}{\omega_i(\Gamma(\alpha)\Gamma(\beta))^2 \sqrt{\gamma_s}} G_{3,3}^{2,3} \left(\frac{\omega_j}{\omega_i} \middle| \begin{smallmatrix} 0,1-\alpha,1-\beta \\ \alpha-1,\beta-1,0 \end{smallmatrix} \right) \right)^{N_r}. \quad (23)$$

For N_t equiprobable TXs, using the union bound technique [24] the probability of correctly detecting the TX index conditioned on a correctly detected pulse position is:

$$\begin{aligned} P_{c,tx} &\leq 1 - \frac{1}{N_t} \sum_{j=1}^{N_t} \sum_{\substack{i=1 \\ i \neq j}}^{N_t} \text{APEP}_m^{j \rightarrow i} \\ &= 1 - \frac{1}{N_t} \sum_{j=1}^{N_t} \sum_{\substack{i=1 \\ i \neq j}}^{N_t} \frac{2^{N_r} \Gamma(\frac{N_r+1}{2})}{N_r \Gamma(\frac{N_r}{2})} \left(\frac{\alpha \beta}{\omega_i (\Gamma(\alpha) \Gamma(\beta))^2 \sqrt{\gamma_s}} G_{3,3}^{2,3} \left(\frac{\omega_j}{\omega_i} \middle| \begin{smallmatrix} 0,1-\alpha,1-\beta \\ \alpha-1,\beta-1,0 \end{smallmatrix} \right) \right)^{N_r}. \end{aligned} \quad (24)$$

¹¹⁹ 3.2. Probability of Correct Pulse Position Detection

Considering that the transmitted symbol is sent by activating TX j to transmit a pulse in slot m of the L -PPM signal, the average PEP of detecting slot ℓ instead of slot m , is [17]:

$$\text{APEP}_{m \rightarrow \ell}^j = \frac{1}{2} \int_{\mathbf{h}_j} \text{erfc} \left(\sum_{k=1}^{N_r} \sqrt{\frac{\gamma_s}{2} (\omega_j h_{jk})^2} \right) f_{\mathbf{H}}(\mathbf{h}_j) d\mathbf{h}_j, \quad (25)$$

where $f_{\mathbf{H}}(\mathbf{h}_j)$ is the joint PDF of the $N_r \times 1$ vector of channel coefficients: $\mathbf{h}_j = [h_{j1}, \dots, h_{jN_r}]$. The integral in (25) requires N_r -dimensional integration over the PDF of the channel coefficients, given in (7). To obtain a closed form evaluation, we utilize the approximation [25, (14)]:

$$\text{erfc}(x) \simeq \frac{1}{6} e^{-x^2} + \frac{1}{2} e^{-4x^2/3}. \quad (26)$$

By employing (26), the expression in (25) yields:

$$\text{APEP}_{m \rightarrow \ell}^j \simeq \int_{\mathbf{h}_j} \frac{1}{12} e^{-\sum_{k=1}^{N_r} \frac{\gamma_s}{2} (\omega_j h_{jk})^2} f_{\mathbf{H}}(\mathbf{h}_j) d\mathbf{h}_j + \int_{\mathbf{h}_j} \frac{1}{4} e^{-\frac{4}{3} \sum_{k=1}^{N_r} \frac{\gamma_s}{2} (\omega_j h_{jk})^2} f_{\mathbf{H}}(\mathbf{h}_j) d\mathbf{h}_j. \quad (27)$$

Since the channel coefficients $\{h_{jk}\}_{k=1}^{N_r}$ are independent, then (27) can be expressed as:

$$\text{APEP}_{m \rightarrow \ell}^j \simeq \frac{1}{12} \prod_{k=1}^{N_r} \int_0^\infty e^{-\frac{\gamma_s}{2} (\omega_j h_{jk})^2} f_H(h_{jk}) dh_{jk} + \frac{1}{4} \prod_{k=1}^{N_r} \int_0^\infty e^{-\frac{2\gamma_s}{3} (\omega_j h_{jk})^2} f_H(h_{jk}) dh_{jk}. \quad (28)$$

By applying (7) in (28), and expressing the exponential function in terms of the Meijer G-function [21, (8.4.3.1)]:

$$e^{-x} = G_{0,1}^{1,0} \left(x \middle| \begin{smallmatrix} 0 \\ 0 \end{smallmatrix} \right), \quad (29)$$

the expression in (28) becomes:

$$\begin{aligned} \text{APEP}_{m \rightarrow \ell}^j &\simeq \frac{1}{12} \prod_{k=1}^{N_r} \frac{\alpha \beta}{\Gamma(\alpha) \Gamma(\beta)} \int_0^\infty G_{0,1}^{1,0} \left(-\frac{\gamma_s (\omega_j h_{jk})^2}{2} \middle| \begin{smallmatrix} 0 \\ 0 \end{smallmatrix} \right) G_{0,2}^{2,0} \left(\alpha \beta h_{jk} \middle| \begin{smallmatrix} \alpha-1, \beta-1 \\ \alpha-1, \beta-1 \end{smallmatrix} \right) dh_{jk} \\ &\quad + \frac{1}{4} \prod_{k=1}^{N_r} \frac{\alpha \beta}{\Gamma(\alpha) \Gamma(\beta)} \int_0^\infty G_{0,1}^{1,0} \left(-\frac{2\gamma_s (\omega_j h_{jk})^2}{3} \middle| \begin{smallmatrix} 0 \\ 0 \end{smallmatrix} \right) G_{0,2}^{2,0} \left(\alpha \beta h_{jk} \middle| \begin{smallmatrix} \alpha-1, \beta-1 \\ \alpha-1, \beta-1 \end{smallmatrix} \right) dh_{jk}. \end{aligned} \quad (30)$$

The relation in [21, (2.24.1.1)] is then used to evaluate the integration of the product of two Meijer-G terms in (30), and the solution which results is expressed as:

$$\text{APEP}_{m \rightarrow \ell}^j \simeq \frac{1}{12} \left[\frac{2^{(\alpha+\beta)}}{(4\pi)\Gamma(\alpha)\Gamma(\beta)} G_{4,1}^{1,4} \left(-\frac{8(\omega_j)^2 \gamma_s}{(\alpha\beta)^2} \middle| \frac{1-\alpha}{2}, 1-\frac{\alpha}{2}, \frac{1-\beta}{2}, 1-\frac{\beta}{2}, 0 \right) \right]^{N_r} + \frac{1}{4} \left[\frac{2^{(\alpha+\beta)}}{(4\pi)\Gamma(\alpha)\Gamma(\beta)} G_{4,1}^{1,4} \left(-\frac{32(\omega_j)^2 \gamma_s}{3(\alpha\beta)^2} \middle| \frac{1-\alpha}{2}, 1-\frac{\alpha}{2}, \frac{1-\beta}{2}, 1-\frac{\beta}{2}, 0 \right) \right]^{N_r}. \quad (31)$$

Using the union bound technique, the probability of correctly detecting the pulse position is given by:

$$P_{\text{c,ppm}} \leq \frac{1}{N_t} \sum_{j=1}^{N_t} \left(1 - [(L-1) \times \text{APEP}_{m \rightarrow \ell}^j] \right). \quad (32)$$

Finally, the expressions (24) and (32) are substituted into (8) to obtain the upper bound on the asymptotic symbol error probability of SPPM transmission in atmospheric turbulence channels.

4. Results and Discussions

The results of the performance evaluation of the SPPM technique over FSO channels are presented in this section. In all cases, except where otherwise stated, equal weights, i.e., $\{\omega_j\}_{j=1}^{N_t} = 1$, are used. The values of α and β used for each turbulence regime are given in Table 1.

Without any loss of generality, considering the SPPM configuration with $N_t = 2$, $N_r = 4$ and $L = [2, 8]$, the plots of the SER versus SNR per bit, γ_b , under weak and strong AT conditions are shown in Figure 2. Similar error performance plots for the case of $N_t = 4$ are depicted in Figure 3. It can be observed from Figure 2 and Figure 3 that the derived upper bound on the asymptotic SER of SPPM in AT is closely matched by the simulation results. The error performance plot for moderate AT conditions is similar to that of the strong AT, and hence for clarity, the plot for moderate AT is not included. The reason for the SER values being greater than 1, as well as the slight deviations observed between the theoretical and simulation results for $\text{SER} > 10^{-2}$, is due to the union bound technique used in the analysis. Indeed, the closed form expression obtained in Section 3 can be used to study the performance of SPPM in outdoor Gamma-Gamma fading channels without performing computationally intensive Monte-Carlo simulations. In addition, using the PDF of the difference between two weighted GG RVs in Section 3, the framework can be extended to explore the performance of other variants of the OSM technique, such as spatial pulse amplitude modulation (SPAM) and generalised SPPM (GSPPM), in FSO channels. For instance, to extend the framework to study the SPAM scheme, pulse amplitude modulation (PAM) is used instead of the PPM scheme, and the transmit power weights, ω , designed for creating power imbalance in this paper, will then represent the different intensity levels of the PAM scheme.

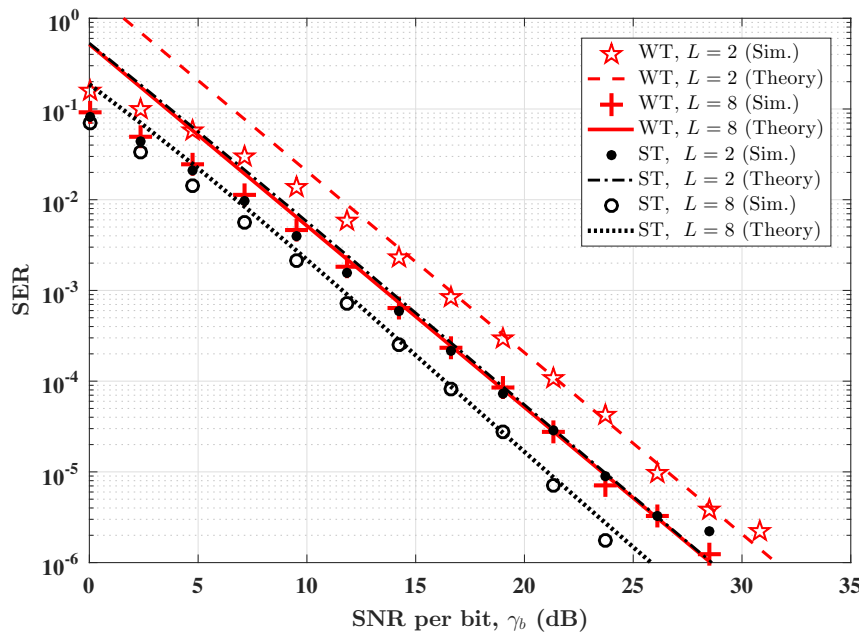


Figure 2. Error performance of SPPM in weak and strong AT conditions. $N_t = 2$, $N_r = 4$ and $L = [2, 8]$. ST: Strong AT and WT: Weak AT.

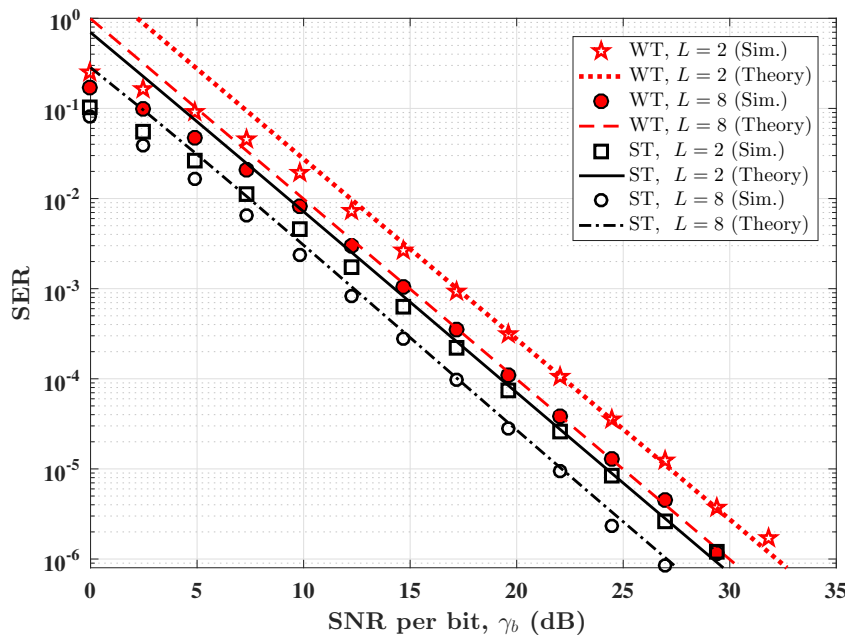


Figure 3. Error performance of SPPM in weak and strong AT conditions. $N_t = 4$, $N_r = 4$ and $L = [2, 8]$. ST: Strong AT and WT: Weak AT.

Using $N_t = 4$, $N_r = 4$ and $L = 8$, the SNR required to achieve a representative SER of 10^{-5} under different AT regimes is depicted in Figure 4. For the case of equal transmit power weights, i.e., $\{\omega_j\}_{j=1}^{N_t} = 1$, it is observed that the SNR required under moderate to strong AT conditions is smaller compared to weak AT cases. As an example, under weak ($\sigma_l^2 = 0.2$), moderate ($\sigma_l^2 = 1.6$) and strong ($\sigma_l^2 = 3.5$) AT regimes, the required SNR is about 24.5 dB, 22 dB and 22.3 dB respectively. This observation can be attributed to the fact that as the AT strength increases from the weak to strong, the distribution of the fading coefficients spreads out more, and the range of possible values of the coefficients increases [1]. Since SPPM, like other OSM schemes, thrives on having distinct channel

coefficients, then a better performance is expected under moderate to strong AT compared to weak AT. However, we also note that as the AT strength increases, the effective SNR of the received signal also decreases due to fading. This explains the slight increase in SNR requirements (albeit, less than 0.7 dB) observed under strong AT compared to moderate AT. Typically, the error performance of OSM schemes is dependent on both the individual values of the channel coefficients as well as the difference between them [17,26], as expressed by (25) and (9) respectively.

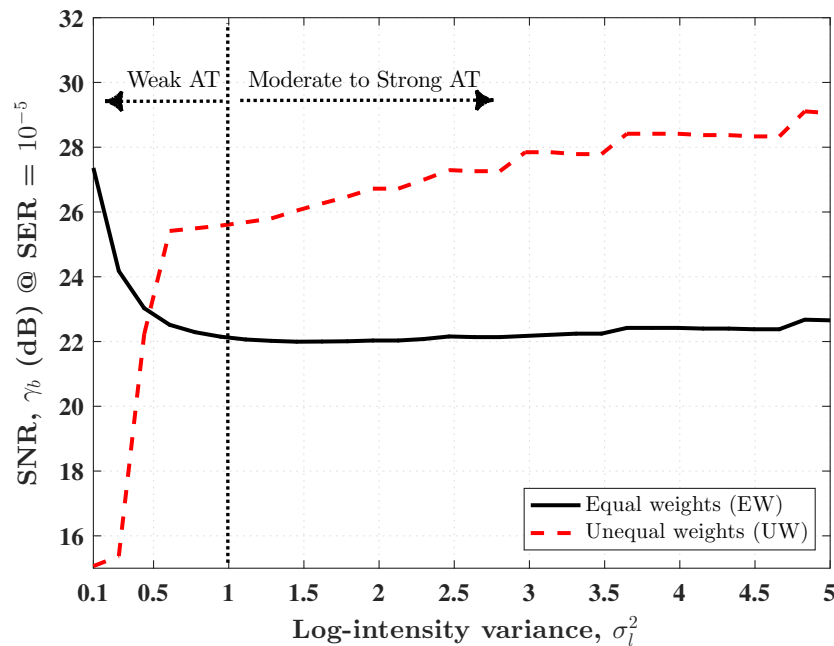


Figure 4. Performance under varying AT regime. SNR required to achieve SER of 10^{-5} for SPPM configuration: $N_t = 4$, $L = 8$.

Furthermore, the system performance under weak AT conditions can be improved by applying unequal power allocation (PA) to make the TXs more distinguishable at the receiver. That is, the optical sources transmit at different peak powers. To keep the the average optical power constant, total emitted power is re-distributed by reducing the power of some TXs and assigning the surplus optical power to the other TXs. The optical PA factor ρ , $0 < \rho \leq 1$, is used to generate the transmit power weights as [27]:

$$\omega_j = N_t \frac{\rho^{j-1}}{\sum_{j=1}^{N_t} \rho^{j-1}} \quad \text{for } j = 1, \dots, N_t. \quad (32)$$

When the TXs are arranged in ascending order of their weights, ρ is the ratio of the smaller to the bigger weights assigned to a pair of consecutive TXs. The higher the value of ρ , the bigger the relative difference in the transmit power weights assigned to each TX. The value of ρ that is applied is dependent on the severity of the channel gain similarity as well as the received SNR of the transmitted digital signal modulation. As an example, for $N_t = 4$ by setting $\rho = 1$, $\rho = 0.5$ and $\rho = 0.25$, we obtain the weights as $\{\omega_j\}_{j=1}^{N_t} = [1, 1, 1, 1]$, $\{\omega_j\}_{j=1}^{N_t} = [2.13, 1.07, 0.53, 0.27]$ and $\{\omega_j\}_{j=1}^{N_t} = [3.01, 0.75, 0.19, 0.05]$ respectively. Considering the case of $\rho = 0.5$, Figure 4 shows that under weak AT ($\sigma_t^2 \leq 0.5$), by using unequal weights, a reduction in the SNR requirement is achieved compared to using equal weights. However, since the total transmit power is kept constant, by applying the PA technique, the SNR values of signals with the smaller weights are further reduced in addition to the attenuation caused by AT. This effect can be seen in the performance deterioration observed for $\sigma_t^2 > 0.5$ in Figure 4. The unequal PA technique is largely effective when the channel coefficients are less distinct, as in weak AT. To achieve the best results, the relationship between PA and error performance must be optimised

170 by considering the impact of PA technique on the detection of transmitter index and the transmitted
 171 digital signal modulation.

172 The SPPM scheme, as for OSM techniques in general, utilize multiple optical sources at the
 173 transmitter to convey additional information bits, thereby providing increased throughput. Therefore,
 174 to achieve diversity gain, particularly in the dynamic FSO channels, multiple PDs can be employed
 175 at the receiver. Considering an SPPM configuration with $N_t = 4$ and $L = 8$, the plots of SER against
 176 γ_b with multiple PD, under weak and strong AT conditions, are provided in Figure 5. As observed
 177 in the Figure 5, as the number of PDs increases, the SNR required to attain a specified SER reduces
 178 across all the turbulence regimes. For example, under strong AT conditions, the SNR required to attain
 179 an SER of 10^{-5} is reduced by a factor of about 24 dB (from 46 dB to 22 dB) when number of PDs is
 180 increased from 2 to 4. In fact, the diversity order, obtained from the asymptotic slope of the SER curve
 181 (in log-log scale) in the high SNR regime [28], is $d_o = N_r/2$, under all AT conditions. For instance,
 182 in Figure 5, under weak AT conditions, for $N_r = 2$, the SER at SNR of 40 dB and 50 dB is 10^{-4} and
 183 10^{-5} respectively. Thus, $d_o = -\log(10^{-5}/10^{-4})/\log(10^5/10^4) = 1$. Also, for $N_r = 4$, the SER at SNR
 184 of 20 dB and 30 dB is 10^{-4} and 10^{-6} respectively, and $d_o = -\log(10^{-6}/10^{-4})/\log(10^3/10^2) = 2$. Note
 185 that in computing the values of d_o , the SNR values have been converted from the decibel scale to the
 186 linear scale. Similar results can be obtained from the other error performance plots in Figure 5. Using
 187 multiple PDs improves the robustness of the SPPM system to turbulence-induced channel fading.

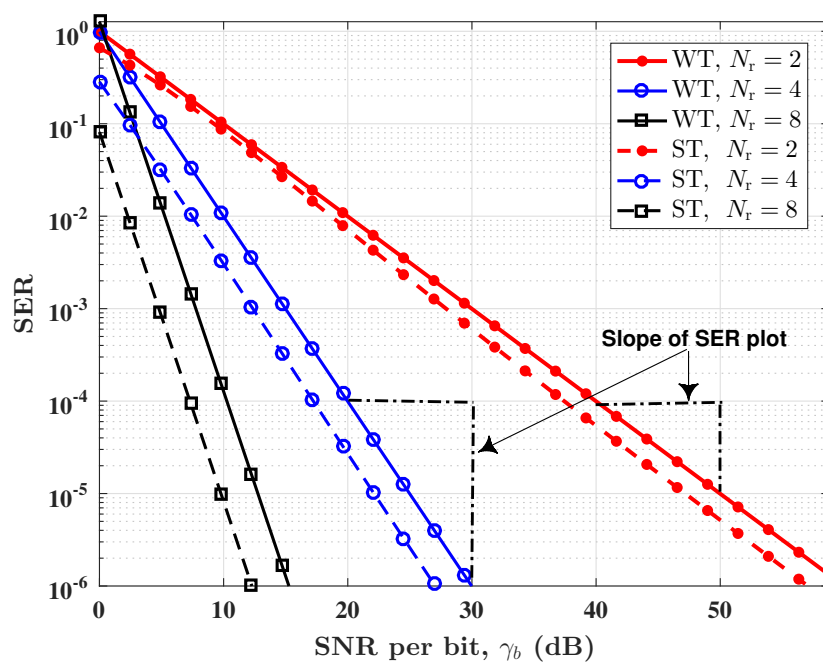


Figure 5. SNR required to achieve $SER = 10^{-5}$, using varying number of PDs. SPPM configuration: $N_t = 4$, $L = 8$.

188 The performance comparison of SPPM with other MIMO schemes in terms of energy and spectral
 189 efficiencies is illustrated in Figure 7 and Figure 6 respectively. The SPPM is compared with SSK,
 190 repetition coded PPM (RC-PPM) and spatial multiplexed PPM (SMX-PPM) schemes. For an energy
 191 efficiency comparison, we estimate the SNR required to achieve an SER of 10^{-5} . We consider $N_t = 4$,
 192 and the same average transmitted optical power is used for all techniques. Figure 6 shows that the
 193 maximum spectral efficiency, η_{spec} , of SPPM (using $L = 2$) exceeds that of RC-PPM by 1 bits/s/Hz. The
 194 value of η_{spec} is higher for SSK compared to SPPM because the pulse duration in SSK is L times longer
 195 than that of SPPM, though SPPM transmits more bits/symbol. As expected, due to the multiplexing
 196 gains of SMX-PPM, its η_{spec} is higher than that of SPPM. However, as shown in Figure 7, the SPPM
 197 scheme achieves up to 15.4 dB (using $L = 2$) savings in SNR compared to SMX-PPM. This is because, in

198 SPPM, only one TX is activated in a given symbol duration, whereas, for SMX-PPM all the TXs are
 199 activated concurrently and their emitted intensities are divided by a factor of N_t in order to achieve
 200 equal average transmitted optical power. Moreover, the single-transmitter activation in SPPM prevents
 201 interchannel interference which reduces the complexity of the detection algorithms. Compared to SSK,
 202 the SPPM schemes achieves up 35 dB savings in SNR due to use of PPM which gives a shorter pulse
 203 duration. As L increases, the energy saving by SPPM, in terms of SNR, increases. This highlights how
 204 the power efficiency benefits of PPM is harnessed in SPPM.

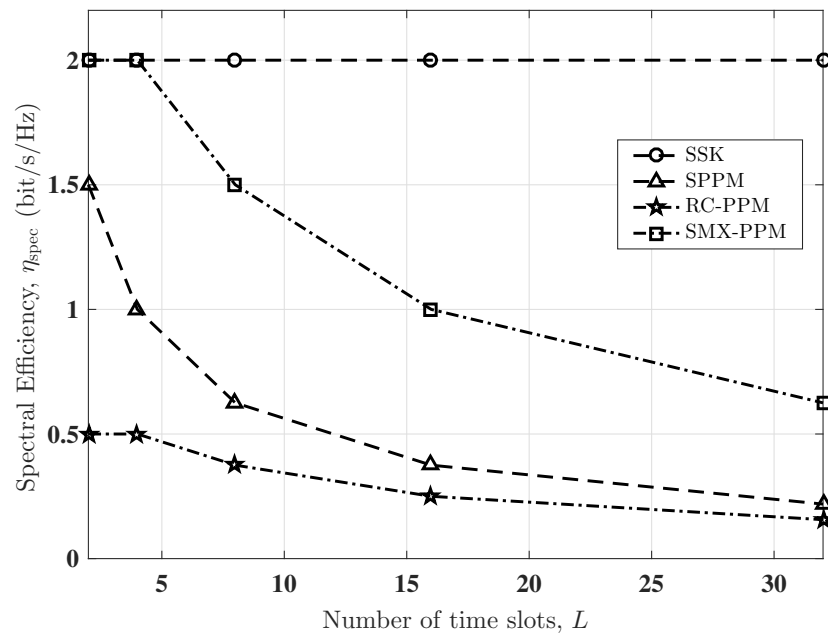


Figure 6. Spectral efficiency comparison of SPPM with SSK, RC-PPM and SMX-PPM for different values of L , using $N_t=4$, and under strong AT condition.

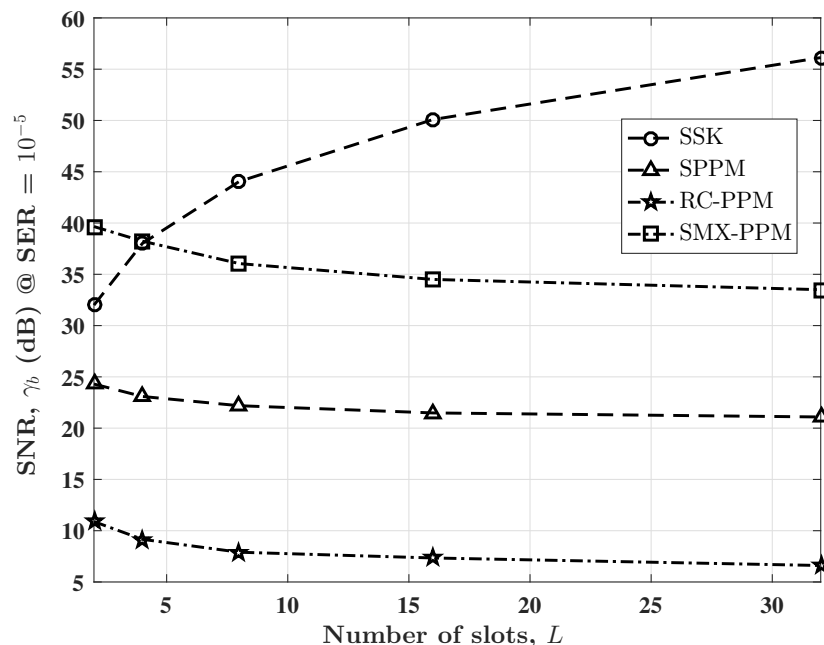


Figure 7. Energy efficiency comparison of SPPM with SSK, RC-PPM and SMX-PPM for different values of L , using $N_t=4$, $N_r=4$, and under strong AT condition.

205 5. Conclusion

206 The theoretical upper bound on the asymptotic SER for SPPM based FSO system has been
207 presented in different atmospheric turbulence regimes from weak to strong. The turbulence-induced
208 fading in the FSO channel is modelled by the widely adopted Gamma-Gamma distribution. Our
209 analytical framework provides a closed-form expression for the SER, and it can be extended to explore
210 the performance of other OSM schemes in FSO channels. As the AT strength increases from weak
211 to strong, the channel fading coefficients become more dispersed and differentiable. Thus, a better
212 error performance is observed under moderate-to-strong AT compared to weak AT. The performance
213 in weak AT can however be improved by applying unequal transmit power allocation to make the
214 FSO links more identifiable at the receiver. Spatial diversity has been considered at the receiver to
215 mitigate irradiance fluctuation and improve the robustness of the SPPM-FSO system to channel fading.
216 The diversity order is obtained as half of the number of detectors employed at the receiver. In terms
217 of energy and spectral efficiencies, the performance of SPPM is compared with conventional MIMO
218 techniques such as repetition coding and spatial multiplexing.

219 **Author Contributions:** “conceptualization, H.O, and W.P; formal analysis, H.O. and W.P.; investigation, H.O, J.T.,
220 and W.P.; software, H.O.; writing—original draft preparation, H.O; writing—review and editing, J.T. and W.P.;
221 supervision, J.T. and W.P.”

222 **Funding:** This work is supported by the Petroleum Technology Development Fund (PTDF) of the Federal
223 government of Nigeria.

224 **Conflicts of Interest:** “The authors declare no conflict of interest.”

225 References

- 226 1. Ghassemlooy, Z.; Popoola, W.; Rajbhandari, S. *Optical Wireless Communications: System and Channel*
227 *Modelling with Matlab®*; CRC Press, 2012.
- 228 2. Khalighi, M.A.; Uysal, M. Survey on Free Space Optical Communication: A Communication Theory
229 Perspective. *IEEE Communications Surveys & Tutorials* **2014**, *16*, 2231–2258.
- 230 3. Gappmair, W.; Hranilovic, S.; Leitgeb, E. Performance of PPM on Terrestrial FSO Links with Turbulence
231 and Pointing Errors. *IEEE Communications Letters* **2010**, *14*.
- 232 4. Bayaki, E.; Schober, R.; Mallik, R.K. Performance Analysis of MIMO Free-space Optical Systems in
233 Gamma-Gamma Fading. *IEEE Transactions on Communications* **2009**, *57*, 3415–3424.
- 234 5. Popoola, W.O.; Ghassemlooy, Z. BPSK Subcarrier Intensity Modulated Free-space Optical Communications
235 in Atmospheric Turbulence. *Journal of Lightwave technology* **2009**, *27*, 967–973.
- 236 6. Bhatnagar, M.R.; Ghassemlooy, Z. Performance Analysis of Gamma–gamma Fading FSO MIMO Links
237 With Pointing Errors. *Journal of Lightwave Technology* **2016**, *34*, 2158–2169.
- 238 7. Song, X.; Cheng, J. Subcarrier Intensity Modulated MIMO Optical Communications in Atmospheric
239 Turbulence. *Journal of Optical Communications and Networking* **2013**, *5*, 1001–1009.
- 240 8. Mesleh, R.Y.; Haas, H.; Sinanovic, S.; Ahn, C.W.; Yun, S. Spatial Modulation. *IEEE Transactions on Vehicular*
241 *Technology* **2008**, *57*, 2228–2241.
- 242 9. Mesleh, R.; Elgala, H.; Haas, H. Optical Spatial Modulation. *IEEE/OSA Journal of Optical Communications*
243 *and Networking* **2011**, *3*, 234–244. doi:10.1364/JOCN.3.000234.
- 244 10. Jaiswal, A.; Bhatnagar, M.R.; Jain, V.K. Performance Evaluation of Space Shift Keying in Free-space Optical
245 Communication. *IEEE/OSA Journal of Optical Communications and Networking* **2017**, *9*, 149–160.
- 246 11. Abaza, M.; Mesleh, R.; Mansour, A.; others. Performance Analysis of Space-Shift Keying over
247 Negative-Exponential and Log-normal FSO Channels. *Chinese Optics Letters* **2015**, *13*, 051001–051001.
- 248 12. Jaiswal, A.; Bhatnagar, M.R.; Jain, V.K. BER Analysis of Optical Space Shift Keying in Atmospheric
249 Turbulence Environment. *Communication Systems, Networks and Digital Signal Processing (CSNDSP)*,
2016 10th International Symposium on. IEEE, 2016, pp. 1–6.
- 250 13. Özbilgin, T.; Koca, M. Optical Spatial Modulation Over Atmospheric Turbulence Channels. *Journal of*
251 *Lightwave Technology* **2015**, *33*, 2313–2323.

253 14. Peppas, K.P.; Mathiopoulos, P.T. Free-Space Optical Communication With Spatial Modulation and Coherent
254 Detection Over H-K Atmospheric Turbulence Channels. *Journal of Lightwave Technology* **2015**, *33*, 4221–4232.

255 15. Jaiswal, A.; Bhatnagar, M.R.; Jain, V.K. Performance of Optical Space Shift Keying Over Gamma–Gamma
256 Fading With Pointing Error. *IEEE Photonics Journal* **2017**, *9*, 1–16.

257 16. Odeyemi, K.O.; Owolawi, P.A.; Srivastava, V.M. Optical Spatial Modulation over Gamma–Gamma
258 Turbulence and Pointing Error Induced Fading Channels. *Optik-International Journal for Light and Electron
259 Optics* **2017**, *147*, 214–223.

260 17. Popoola, W.O.; Poves, E.; Haas, H. Spatial Pulse Position Modulation for Optical Communications. *Journal
261 of Lightwave Technology* **2012**, *30*, 2948–2954.

262 18. Andrews, L.C.; Phillips, R.L. *Laser Beam Propagation Through Random Media*; Vol. 152, SPIE press Bellingham,
263 WA, 2005.

264 19. Kahn, J.M.; Barry, J.R. Wireless Infrared Communications. *Proceedings of the IEEE* **1997**, *85*, 265–298.

265 20. Andrews, L.C.; Phillips, R.L.; Hopen, C.Y. *Laser Beam Scintillation with Applications*; Vol. 99, SPIE press,
266 2001.

267 21. Prudnikov, A.P.; Brychkov, Y.A.; Marichev, O.I. *Integrals and Series, Volume 3: More special functions*; Gordon
268 and Breach, 1990.

269 22. Osche, G.R. *Optical Detection Theory for Laser Applications*; Wiley Hoboken, NJ, 2002.

270 23. Ng, E.W.; Geller, M. A Table of Integrals of the Error Function. *J. Research Natl. Bureau of Standards* **1968**,
271 *73B*, 149–163.

272 24. Proakis, J.; Salehi, M. *Digital Communications*, 5 ed.; McGraw-Hill, 2008.

273 25. Chiani, M.; Dardari, D.; Simon, M.K. New Exponential Bounds and Approximations for the Computation
274 of Error Probability in Fading Channels. *IEEE Transactions on Wireless Communications* **2003**, *2*, 840–845.

275 26. Zhang, X.; Dimitrov, S.; Sinanovic, S.; Haas, H. Optimal Power Allocation in Spatial Modulation OFDM for
276 Visible Light Communications. Vehicular Technology Conference (VTC Spring), 2012 IEEE 75th. IEEE,
277 2012, pp. 1–5.

278 27. Fath, T.; Haas, H. Performance Comparison of MIMO techniques for Optical Wireless Communications in
279 Indoor Environments. *IEEE Transactions on Communications* **2013**, *61*, 733–742.

280 28. Lozano, A.; Jindal, N. Transmit Diversity vs. Spatial Multiplexing in Modern MIMO Systems. *IEEE
281 Transactions on Wireless Communications* **2010**, *9*.